Hard Magnetic Materials

Microfabricated Electro-Permanent Magnets Using AlNiCo and CoPt

Yuzheng Wang, Beatriz Y. Jimenez, Connor S. Smith, Adrian A. Rendon-Hernandez, Joseph Samman, and David P. Arnold

Interdisciplinary Microsystems Group, Department of Electrical and Computer Engineering, University of Florida, Gainesville, FL 32611, USA

Received 24 Feb 2021, revised 26 May 2021, accepted 30 Jun 2021, published 26 Jul 2021, current version 30 Aug 2021.

Abstract—This letter demonstrates the fabrication and characterization of externally switchable electro-permanent magnets (EPMs) microfabricated on silicon wafers. Each EPM comprises a thick-film bilayer of electroplated cobalt-platinum as the hard magnetic phase and screen-printed aluminum-nickel-cobalt/polydimethylsiloxane composite as the soft magnetic phase. The selected magnetic materials and corresponding fabrication methods are compatible with standard semiconductor processes, which enable batch fabrication capability for low-cost and system-on-chip integration. An ON/OFF magnetic moment ratio of 265 is achieved for the miniaturized 3.6 mm × 3.6 mm × 0.3 mm EPM devices by varying the volume ratio of the constituent materials. Scanning electron microscopy and vibrating sample magnetometry are used to characterize the microscopic structure and magnetic performance of the fabricated devices, respectively.

Index Terms—Hard magnetic materials, electro-permanent magnets, electrodeposition, CoPt, screen-printing.

I. INTRODUCTION

The electro-permanent magnet (**EPM**) has been curiously explored in biomedical, microrobotic, and microfluidic devices for its unique switchable magnetic behavior [Tugwell 2014, Kriengkomol 2016, Padovani 2016, Gholizadeh 2019]. Distinct from a traditional electromagnet or permanent magnet, which either requires a continuous power supply to produce magnetic field or lacks the capability of proactively terminating the field, an EPM consumes zero static power to generate a magnetic field and only takes an instant pulse of an external magnetic field to achieve ON/OFF controllability [Nerses Knaian 2010]. Typically, this behavior is attributed to the two magnetic materials used in the EPM: a high-coercivity "hard" magnetic phase and a relatively low-coercivity "soft" magnetic phase [Velez 2018]. For the ON state, the two phases are magnetized in the same direction, and the EPM generates a net external magnetic field like a permanent magnet. After applying a short pulse of magnetic field to reverse the magnetization direction of the soft phase (usually generated by a pulsed current through a coil), the fields generated by the two phases are mostly self-contained inside the EPM.

While most previously reported EPMs make use of manually assembled bulk magnetic components, the goal of this letter is to develop highly miniaturized EPMs with simplified device architecture. The manufacturing approach employs batch-fabrication methods to deposit patterned magnetic films. The long-term goal is to integrate these ultrasmall EPMs into more complex magnetic microsystems, such as microfluidics, microrobotics, or more. This letter reports the detailed fabrication process of an innovative miniaturized EPM architecture as well as the characterizations of the materials and the EPM magnetic performance.

Corresponding author: Yuzheng Wang (e-mail: wangyz0218@ufl.edu).
Digital Object Identifier 10.1109/LMAG.2021.3099454

II. DEVICE DESIGN AND RATIONALE

When designing an EPM, it is desirable to achieve a large ON magnetic moment and a small OFF magnetic moment while using the smallest possible magnetic field for switching between the states. This requires high-remanence permanent magnetic materials and a large difference in coercivity between the hard and soft phases. Specifically, the high-remanence is attributed to a large magnetic moment at the ON state, and the low-coercivity soft phase enables a low minimum switching field. In addition, less material is needed to fabricate an EPM by the introduction of high-remanence magnetic materials, which is beneficial for reducing the size and weight of the device. While there are many different material choices, here we use electrodeposited equiatomic cobalt-platinum (CoPt) as the hard phase, and screen-printed aluminum-nickel-cobalt (AlNiCo)/polydimethylsiloxane (PDMS) composite as the soft phase. These materials and methods facilitate batch fabrication of relatively thick films (tens of micrometers) without expensive film deposition tools.

Miniaturized EPM devices are fabricated using a simple stacked bilayer architecture, with an electroplated CoPt disc on the bottom, followed by a screen-printed AlNiCo/PDMS on top [Ito 2007, Xing 2013, Zhou 2014]. The magnets are deposited into circular geometry, which 1) allows the EPM to be magnetized in any in-plane direction and 2) eliminates stress concentrations that commonly occur in the corners of electrodeposited films. Electrodeposition and screen-printing are selected for their relatively simple, yet batch fabrication capability, and for compatibility with other standard semiconductor processes. A "purist" may argue that the structure is not technically an EPM, since it does not contain an integrated coil winding. However, for many emerging applications, particularly at small physical scales, the switching field may be generated by an external structure (not contained within the magnetic layers). Hence, in this letter, we will use the term EPM, even though the structure lacks an integrated winding.

Fig. 1 presents a three-dimensional finite-element simulation

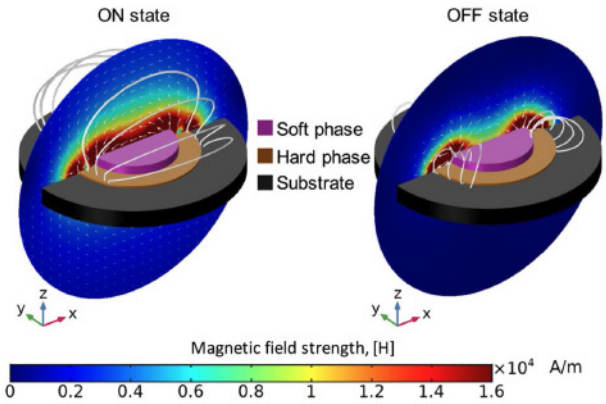

Fig. 1. Finite-element simulation (COMSOL Multiphysics) of the microfabricated EPM comprising electroplated CoPt (hard phase, 55 μm thick, 3.6 mm diameter, 0.24 mA·m^2) and screen-printed AlNiCo/PDMS composite (soft phase, 250 μm thick, 2.4 mm diameter, 0.26 mA·m^2) on a silicon substrate.

(COMSOL Multiphysics) of the microfabricated EPM with a diameter of 3.6 mm and a total thickness of 0.3 mm. The design here does not use any high-permeability magnetic flux guiding structures, as commonly used in larger EPM devices. By controlling the magnetic properties and dimensions of the two phases, a design goal of the microfabricated EPM is that the two phases exhibit approximately equal magnetic moments. Consequently, when the two phases are counter-magnetized, the combined structure will exhibit zero net magnetic moment [Diller 2012]. As will be shown, the EPM is switched between ON and OFF states by applying a magnetic field pulse of approximately 400–700 kA/m (0.5–0.8 T). This letter focuses on the detailed fabrication process of an innovative miniaturized EPM architecture as well as the characterizations of the materials and the EPM magnetic performance.

III. DEVICE FABRICATION

The overall fabrication process is introduced in Fig. 2. Starting from a silicon wafer, the CoPt magnet is first electrodeposited inside the photolithographically patterned electroplating mold and annealed to induce hard magnetic properties. Then, the AlNiCo particles/PDMS mixture is screen-printed on top of the CoPt layer and cured within the external field for preferentially aligning the particles.

A. Electrodeposition of CoPt Magnets

The fabrication of the equiatomic CoPt magnetic structures follows previously reported procedures [Wang 2019b, 2020]. Silicon wafers with 1000 nm thermal oxide are used as the starting substrate. For electroplating, the functional layer stacks consist of two 25 nm Cr adhesion improving layers, one 50 nm TiN diffusion barrier, one 500 nm Cu conductive seed layer, and one 50 nm Ti sacrificial layer, all deposited via sputtering. A 60 μm thick SU-8 2050 photoresist mold is deposited and patterned with 3.6 mm diameter circular apertures for the electrodeposition of CoPt magnets [Wang 2019a]. Just prior to the electrodeposition, the titanium layer exposed within the SU-8 mold is quickly etched using diluted hydrofluoric acid (HF:H_20 = 1:10) to expose the Cu seed layer.

The dc electroplating is conducted using a plating bath that contains dinitrodiamine-platinum, cobalt sulfamate, and ammonium citrate serving as the platinum source, cobalt source, and pH buffer/complexing agent, respectively. A deposition rate of ~28 μm/h is achieved at a current density of 400 mA/cm^2 and bath temperature of 50 °C. A variety of CoPt magnets with thicknesses ranging from 14 to 55 μm (0.5–2 h deposition) can be obtained by simply adjusting the duration of deposition, which leads to one method for controlling the total magnetic moment of the CoPt structure. After electroplating, the sacrificial Ti layer is then dissolved using diluted HF to release the SU-8 mold. A postdeposition annealing step is then performed at 700 °C for 30 min in a tube furnace under forming gas atmosphere (5% H_2, 95% N_2) to induce the hard-magnetic properties of the $L1_0$ CoPt with face-centered tetragonal crystal structure [Xiao 2004, Wang 2019b]. Additional attention is required during the designing of process flow when integrating the EPMs to other structures due to this necessary annealing process. It is important to note that the electroplated CoPt films exhibit orthotropic anisotropy and can be magnetized in any in-plane direction with relatively strong remanence.

B. Screen-Printing of AlNiCo/PDMS

After electroplating the patterned discs of CoPt, disc-shaped soft-magnetic structures are screen-printed on top. AlNiCo (SuperMagnetMan) is chosen 1) for its relatively low coercivity (~100 kA/m) enabling a low switching field and 2) for its availability in powder form enabling low-cost screen-printing deposition [Zhou 2014]. Before commencing the screen-printing process, the AlNiCo is mixed with PDMS binder to form the composite material. Various mixing weight ratios ranging from 50:50 to 90:10 (AlNiCo:PDMS) are explored by screen-printing 3.15 mm diameter discs and comparing them side by side, in search of the ideal consistency for screen-printing. The weight ratios below 80:20 exhibit a runny consistency (especially the 50:50 ratio), so the screen-printed structures fail to maintain their shape, whereas the 90:10 ratio possesses a thick consistency, which makes it difficult to spread the mixture over the screen. As a result, the weight ratio is optimized at 85:15 (AlNiCo:PDMS) for all the following screen-printing processes.

To control the shape of the AlNiCo/PDMS composite in the screen-printing process, a mold or screen is required, which is made for process development purposes, in this case by hole-punching a piece of electroplating tape with a thickness of 210 μm. The punched tape is visually aligned and centered under a microscope over the CoPt magnet, and the AlNiCo/PDMS mixture is spread with a blade to fill the hole, ensuring firm contact to the CoPt layer. Then, the tape is carefully peeled off, revealing the screen-printed 250 μm thick AlNiCo layer. To achieve equal magnetic moment between the two magnetic layers, the volume of the AlNiCo layer is adjusted by varying the diameter of the screen-printed AlNiCo rather than the thickness. AlNiCo discs with diameters ranging from 2.4 to 3.6 mm are explored for the optimization of EPM performance.

A curing setup consisting of a heating source and an electromagnet is utilized to align the AlNiCo particles in-plane and cure the PDMS in the screen-printed layer. An electromagnet, powered by a dc power supply, generates a magnetic field of 240 kA/m with the sample placed between the two electromagnet poles. A heat gun placed ~30 cm away from the sample maintains the temperature at 70 °C to polymerize the PDMS within 30 min. Fig. 3 presents a microscope image and

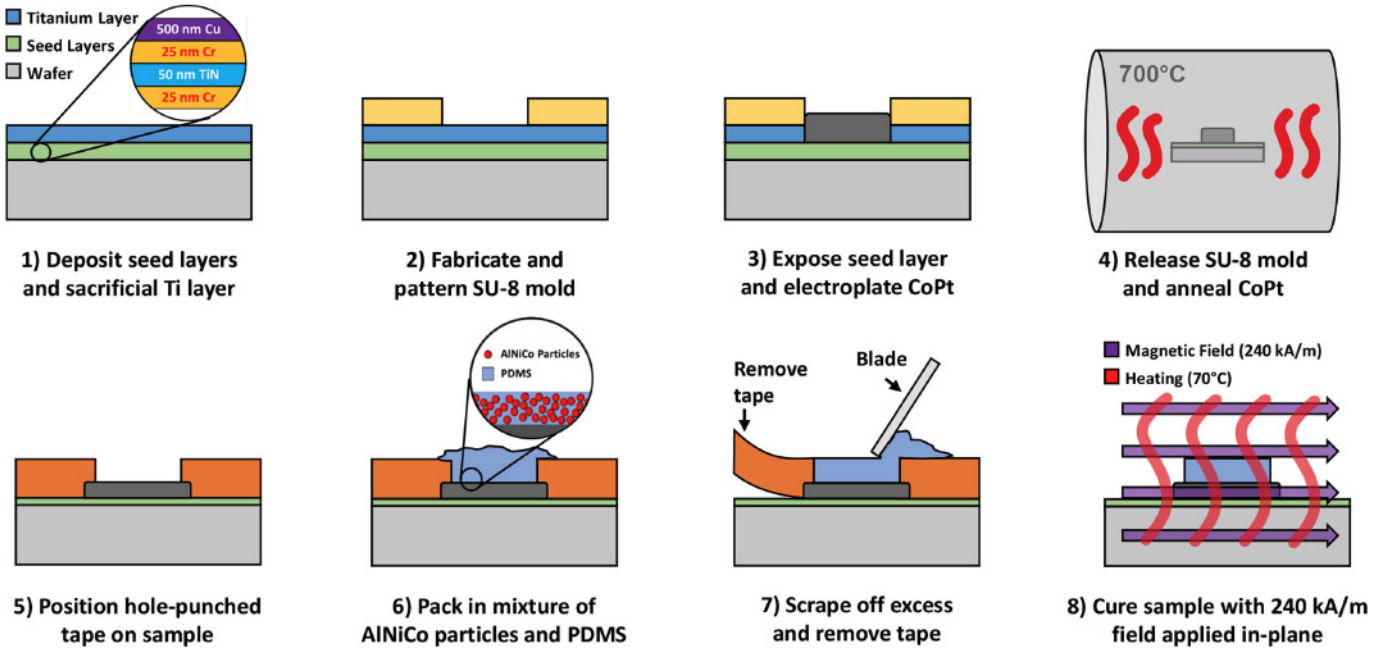

Fig. 2. Complete process flow for EPM fabrication.

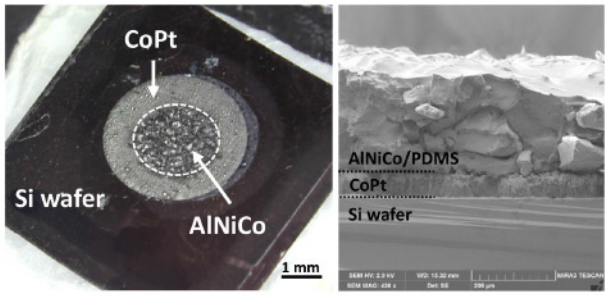

Fig. 3. (Left) Microscope photograph and (right) SEM cross-sectional image of the fabricated EPM device.

an scanning electron microscopy (**SEM**) cross-sectional image of a fabricated EPM.

IV. CHARACTERIZATION

In this section, the characterization results from various analysis techniques are presented. The basic magnetic properties of the materials including coercivity, remanence, and saturation magnetization can be derived from the hysteresis loops measured utilizing a vibrating sample magnetometer (**VSM**). The major hysteresis loop of the EPM will exhibit a distinct, two-phase behavior, due to the decoupled and disparate switching fields of the hard and soft phases. A dc demagnetization (**DCD**) analysis is performed to study the switchability of the EPM devices. The visualization of magnetic field distribution around the EPM using a magnetooptical microscope is also presented.

To begin, all samples are first fully magnetized in-plane using two 4800 kA/m (6 T) pulses, supplied by a pulse magnetizer to fully magnetize the materials prior to the VSM characterization. Fig. 4(a) shows the comparison in hysteresis loops between the electroplated CoPt and the screen-printed AlNiCo particles. The CoPt exhibits strong hard-magnetic properties with coercivity of ~800–900 kA/m, remanence of 480 kA/m, and saturation magnetization of 530 kA/m, which is consistent with the previously reported values [Diller 2012, Wang 2019b, 2020]. In contrast, the relatively softer AlNiCo particles show a coercivity of 100 kA/m, remanence of 290 kA/m, but higher saturation magnetization of 700 kA/m.

As shown in Fig. 4(b), by using these two materials, functional EPM devices can be realized by achieving an equilibrium in the overall magnetic moment. Assuming uniform magnetic properties within a magnet, the magnetic moment is calculated simply by the product of the magnet volume and magnetization. The electrodeposited CoPt magnets deposited for 30 min to 2 h (corresponding to a thickness of 14–55 μm) and screen-printed AlNiCo pellets with a diameter of 2.4 and 3.6 mm are prepared.

Measured hysteresis loops and DCD curves of multiple fabricated EPM devices are presented in Fig. 4(c) and (d). The overall shape of the hysteresis loop can be considered as the superposition of two individual loops of CoPt and AlNiCo, where the significant "kink" appearing at ~800–900 kA/m represents the point of coercivity of the hard CoPt phase. DCD analysis is performed from the saturated state by applying increasing demagnetizing fields to identify the switching field of the fabricated EPM devices. To create a DCD curve, the EPM is always first saturated (conventionally in the negative direction), corresponding to the ON state of the EPM. Next, a demagnetizing or switching field is temporarily applied in opposition to the magnetization direction, and the resultant magnetic moment is recorded. This process is repeated for increasing demagnetizing fields while always starting from the saturated ON state. Fig. 4(d) shows the DCD curves for the various samples. The EPMs start with a saturated negative moment ranging from –0.3 to –0.5 $mA \cdot m^2$, which is the ON state where both the hard and soft phases are magnetized in the same direction. The first switching point found at the externally applied field of ~300 kA/m indicates the field where the polarization of the soft phase is reversed, whereas the hard phase remains unchanged. The EPM is switched from its ON state to OFF state at this point. As the strength of the external field increases, the hard phase will ultimately be flipped at ~800–900 kA/m. Thus, the switching field ranging from 400 to 700 kA/m is identified for the

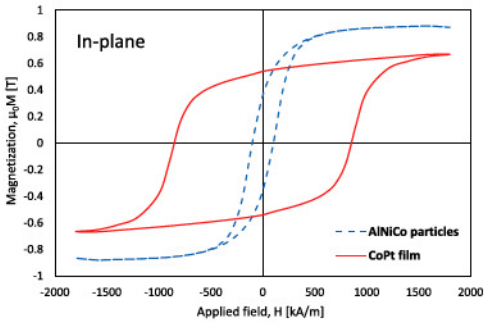

Materials	Diameter [mm]	Thickness [μm]	Magnetic Moment [mA·m²]
CoPt	3.6	14	0.062
	3.6	28	0.12
	3.6	55	0.24
AlNiCo	3.6	250	0.61
	2.4	250	0.26

(b)

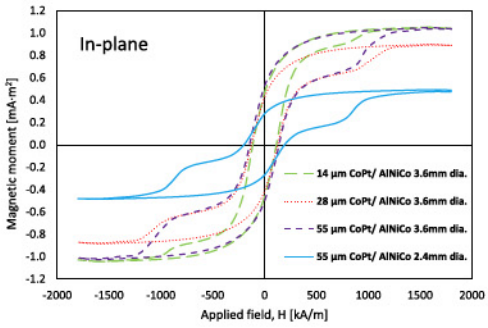

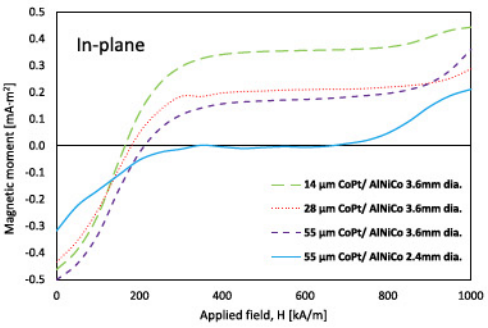

Fig. 4. (a) Hysteresis loops of CoPt magnets and AlNiCo particles. (b) Magnetic moment of various magnetic materials used to fabricate the EPMs. (c) Hysteresis loops and (d) DCD analysis of multiple EPM devices.

fabricated EPM device, indicated by the center "flat" region on the DCD curve. In other words, an opposite pulse switching field ranging anywhere from 400 to 700 kA/m can be applied to the EPM to switch it from the OFF state back to ON state since such a pulse field is only strong enough to flip the polarization of the soft phase.

As the volume ratio of CoPt to AlNiCo increases, the center "flat" region on DCD curves drops closer to the *x*-axis, indicating a smaller net moment while the EPM is OFF. The best performance is achieved for the 55 μm thick, 3.6 mm diameter CoPt magnet and a 250 μm thick, 2.4 mm diameter AlNiCo composite. For this design, an ON/OFF ratio of ~265 is achieved for the EPM by comparing the averaged magnetic moment at the flat region and the *y*-axis interception of the DCD curve. Theoretically, a traditional permanent magnet can be "switched OFF" if applying an external field with the exact value equal to its coercivity. However, obtaining zero moment would be impractical since the magnetization changes rapidly when being forced close to zero by the applied coercive field. Thus, for the EPM, the wide range of switching field instead of a pinpoint enables a huge tolerance in practical applications, where the pulsed switching field may not be precisely controlled.

To better present the magnetic field distribution around the EPM, magnetooptical microscopy (using a magnetooptical indicator film) is used to visualize the surrounding field at ON/OFF states [Patterson 2015]. Fig. 5 shows plan view magnetooptical microscope images for an imaging plane just above the top surface of the EPM (just above the switching AlNiCo layer). The magnetooptical image quantitatively measures the polarity and magnitude of the perpendicular (out-of-plane) magnetic field. The blue color indicates the field is passing down through the imaging plane, and the red color indicates the field is passing up through the plane. Due to the limited field of view of the microscope, two images are imaged separately and stitched together. Fig. 5(a) shows the EPM is fully magnetized to the ON state with a

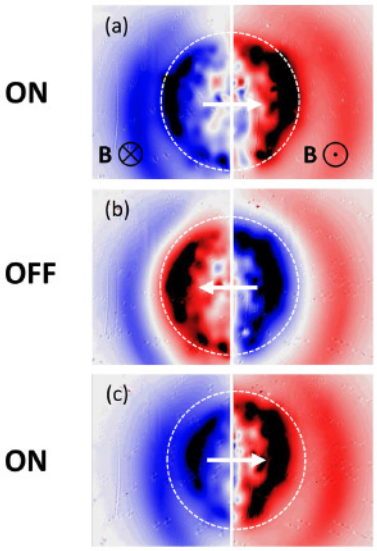

Fig. 5. Magnetooptical microscope images of the fabricated EPM at (a) ON, (b) OFF, and (c) ON state.

relatively strong field generated in the space; here, the top AlNiCo soft phase is magnetized to the right. As shown in Fig. 5(b), the EPM has been switched to the OFF state by an external pulsed field of 500 kA/m; here, the magnetization direction of the AlNiCo has flipped from right to left, whereas the longer range stray field remains in the same polarity, but with weaker amplitude and less "reach." Fig. 5(c) demonstrates the EPM after pulsing back to the ON state by an opposite pulse field with the same strength. The experiments here illustrate that the EPM performs as designed, and the imaging qualitatively matches the stray fields predicted by finite-element modeling (see Fig. 1).

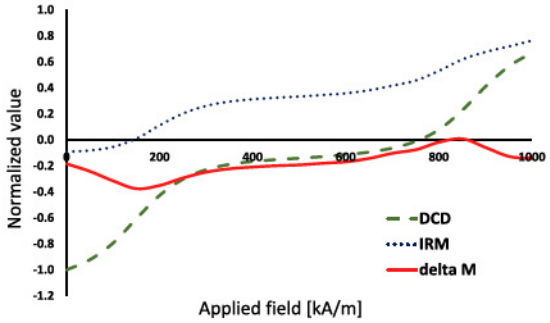

Fig. 6. DCD, IRM, and delta-M measurements of the microfabricated EPM device.

There has been debate as to whether the nanoscale exchange-coupling would affect the magnetic behaviors of our double-layer-structured EPM. A delta-M measurement, which is the most common experimental method for evaluating exchange coupling in magnetic materials, is conducted to either confirm or deny the existence of any observable exchange-coupling in the material stack [Kelly 1989, Wang 2001, van de Veerdonk 2002, Álvarez 2014, Wen 2017]. The delta-M plot combines the data from an isothermal remanent magnetization (**IRM**) and a DCD measurement. In the IRM measurement, the EPM is demagnetized initially by an ac demagnetization field of 1800 kA/m, and then remagnetized by increasing fields ranging from 0 to 1000 kA/m with 50 kA/m increasement (EPM being demagnetized every time between each field step). In the DCD measurement, the EPM is negatively saturated initially by a field of 1800 kA/m, and then positively magnetized by increasing fields ranging from 0 to 1000 kA/m with 50 kA/m increments (EPM being negatively saturated every time between each field step). The delta-M is given by the following relation between two remanence curves:

$$\delta M \;=\; 2 \times M_{\mathrm{IRM}} - 1 - M_{\mathrm{DCD}}$$

where M_{IRM} is the IRM curve and M_{DCD} is the DCD curve. The two curves are normalized to the saturated remanence value. Exchange coupling is identified/confirmed anywhere where the "delta-M" curve exceeds zero. As shown in Fig. 6, a delta-M curve fully below the x-axis within the operating field range indicates no exchange-coupling between two magnetic phases.

V. CONCLUSION

The complete fabrication of miniaturized EPM devices comprising electroplated CoPt magnetic magnets and screen-printed AlNiCo/PDMS composites is demonstrated in this letter. The CoPt magnet is electrodeposited on the silicon wafer at a current density of 400 mA/cm^2 and temperature of 50 °C to obtain a deposition rate of ~28 μm/h. The AlNiCo magnetic particles are mixed with PDMS binder at the optimized weight ratio of 85:15 (AlNiCo:PDMS), enabling the screen-printing on top of the CoPt magnet. The 250 μm thick AlNiCo/PDMS composite is printed and then cured at 70 °C for 30 min with an in-plane magnetic field of 240 kA/m to ensure the preferential alignment of AlNiCo particles. The magnetic moments of the hard and soft phases are balanced by varying the thickness and/or diameter of the deposited phases, ultimately realizing a 3.6 mm × 3.6 mm × 0.3 mm micro-EPM. A maximum ON/OFF magnetic moment ratio of ~265 is achieved with a switching field of 400–700 kA/m. In future efforts, it is ideal to fabricate the two phases with the same diameter to minimize the stray field and explore alternative soft phase materials aiming for lower field required to switch the EPM.

ACKNOWLEDGMENT

This work was supported by the National Science Foundation under Award CMMI-1762700. The authors thank the staff of the UF Engineering Research Service Centers for their assistance in the microfabrication and material characterization.

REFERENCES

Álvarez N, Sallica Leva E, Valente R C, Vásquez Mansilla M, Gómez J, Milano J, Butera A (2014), "Correlation between magnetic interactions and domain structure in A1 FePt ferromagnetic thin films," *J. Appl. Phys.*, vol. 115, 083907, doi: 10.1063/1.4866685.

Diller E, Miyashita S, Sitti M (2012), "Magnetic hysteresis for multi-state addressable magnetic microrobotic control," in *Proc. IEEE/RSJ Int. Conf. Intell. Robots Syst.*, Vilamoura-Algarve, Portugal, pp. 2325–2331, doi: 10.1109/IROS.2012.6386010.

Gholizadeh A, Abbaslou S, Xie P, Knaian A, Javanmard M (2019), "Electronically actuated microfluidic valves with zero static-power consumption using electropermanent magnets," *Sensors Actuators A, Phys.*, vol. 296, pp. 316–323, doi: 10.1016/j.sna.2019.06.037.

Ito S, Chen P, Comte P, Nazeeruddin M K, Liska P, Péchy P, Grätzel M (2007), "Fabrication of screen-printing pastes from TiO_2 powders for dye-sensitised solar cells," *Prog. Photovolt., Res. Appl.*, vol. 15, pp. 603–612, doi: 10.1002/pip.768.

Kelly P E, O'Grady K, Mayo P I, Chantrell R W (1989), "Switching mechanisms in cobalt-phosphorus thin films," *IEEE Trans. Magn.*, vol. 25, pp. 3881–3883, doi: 10.1109/20.42466.

Kriengkomol P, Kamiyama K, Kojima M, Horade M, Mae Y, Arai T (2016), "A new close-loop control method for an inspection robot equipped with electropermanent-magnets," *J. Robot. Mechatronics*, vol. 28, pp. 185–193, doi: 10.20965/jrm.2016.p0185.

Nerses Knaian A (2010), "Electropermanent magnetic connectors and actuators: Devices and their application in programmable matter," Ph.D. dissertation, Dept. Elect. Eng. Comput. Sci., Massachusetts Inst. Technol., Cambridge, MA, USA. [Online]. Available: http://hdl.handle.net/1721.1/60151

Padovani J, Jeffrey S, Howe R (2016), "Electropermanent magnet actuation for droplet ferromicrofluidics," *Technology*, vol. 4, pp. 110–119, doi: 10.1142/S2339547816500023.

Patterson W C, Garraud N, Shorman E E, Arnold D P (2015), "A magneto-optical microscope for quantitative measurement of magnetic microstructures," *Rev. Sci. Instrum.*, vol. 86, 094704, doi: 10.1063/1.4930178.

Tugwell J, Brennan P, O'Shea C, O'Donoghue K, Power T, O'Shea M, Griffiths J, Cahill R, Murphy P (2014), "Electropermanent magnetic anchoring for surgery and endoscopy," *IEEE Trans. Biomed. Eng.*, vol. 62, pp. 842–848, doi: 10.1109/TBME.2014.2366032.

van de Veerdonk R J M, Wu X, Weller D (2002), "Switching field distributions and ΔM measurements for perpendicular media," *IEEE Trans. Magn.*, vol. 38, pp. 2450–2452, doi: 10.1109/TMAG.2002.803589.

Velez C, Tatum L P, Herstein B S, Becker C P, Arnold D P (2018), "Batch-fabrication and characterization of miniaturized axisymmetric electropermanent magnets," *J. Phys., Conf. Ser.*, vol. 1052, 012045, doi: 10.1088/1742-6596/1052/1/012045.

Wang S, Khapikov A F, Brown S, Harrell J W (2001), "Thermal effects on Delta-M measurements in magnetic thin films," *IEEE Trans. Magn.*, vol. 37, pp. 1518–1520, doi: 10.1109/20.950888.

Wang Y, Bowrothu R, Yoon Y K, Arnold D P (2019a), "Patterning of thick electroplated CoPt magnets using SU-8 micromoulds," *Micro Nano Lett.*, vol. 14, pp. 1393–1396, doi: 10.1049/mnl.2019.0287.

Wang Y, Ewing J, Arnold D P (2019b), "Ultra-thick electroplated CoPt magnets for MEMS," *J Microelectromech. Syst.*, vol. 28, pp. 311–320, doi: 10.1109/JMEMS.2018.2888846.

Wang Y, Jimenez B Y, Arnold D P (2020), "100-μm-thick high-energy-density electroplated CoPt permanent magnets," in *Proc. IEEE 33rd Int. Conf. Micro Electro Mech. Syst.*, Vancouver, BC, Canada, pp. 558–561, doi: 10.1109/MEMS46641.2020.9056360.

Wen X, Andrew J S, Arnold D P (2017), "Exchange-coupled hard magnetic Fe-Co/CoPt nanocomposite films fabricated by electro-infiltration," *AIP Adv.*, vol. 7, 056225, doi: 10.1063/1.4976951.

Xiao Q F, Bruck E, Zhang Z D, de Boer F R, Buschow K H J (2004), "Phase transformation and magnetic properties of bulk CoPt alloy," *J. Alloy Compd.*, vol. 364, pp. 64–71, doi: 10.1016/S0925-8388(03)00552-8.

Xing Q, Miller M K, Zhou L, Dillon H M, McCallum R W, Anderson I E, Kramer M J (2013), "Phase and elemental distributions in alnico magnetic materials," *IEEE Trans. Magn.*, vol. 49, pp. 3314–3317, doi: 10.1109/TMAG.2013.2252155.

Zhou L, Miller M K, Lu P, Ke L, Skomski R, Dillon H, Xing Q, Palasyuk A, McCartney M R, Smith D J, Constantinides S, McCallum R W, Anderson I E, Antropov V, Kramer M J (2014), "Architecture and magnetism of alnico," *Acta Mater.*, vol. 74, pp. 224–233, doi: 10.1016/j.actamat.2014.04.044.